

Enhanced entanglement scaling and area-law charge fluctuations in a non-Fermi liquid of composite fermions

Cristian Voinea¹, Songyang Pu^{1,2}, Ajit C. Balam^{3,4} and Zlatko Papić^{1,*}

¹*School of Physics and Astronomy, University of Leeds, Leeds LS2 9JT, United Kingdom*

²*Department of Physics and Astronomy, The University of Tennessee, Knoxville, TN 37996, USA*

³*Institute of Mathematical Sciences, CIT Campus, Chennai 600113, India*

⁴*Homi Bhabha National Institute, Training School Complex, Anushaktinagar, Mumbai 400094, India*

(Dated: July 17, 2024)

The composite fermion Fermi liquid (CFL) state at $\nu=1/2$ filling of a Landau level is a paradigmatic example of a non-Fermi liquid borne out purely by Coulomb interactions. But in what ways is this exotic state of matter precisely different from a Fermi liquid? The entanglement entropy of the CFL state was indeed found to exhibit a significant enhancement compared to free electrons [Shao *et al.*, Phys. Rev. Lett. **114**, 206402 (2015)], which was subsequently ruled out as a finite-size effect by the study of a lattice CFL analogue [Mishmash and Motrunich, Phys. Rev. B **94**, 081110 (2016)]. Moreover, the enhancement was not observed in a quasi-one-dimensional limit of the Coulomb ground state at $\nu=1/2$ [Geraedts *et al.*, Science **352**, 197 (2016)]. Here, we revisit the problem of entanglement scaling in the CFL state realized in a two-dimensional continuum system. Using Monte Carlo evaluation of the second Rényi entropy S_2 for the CFL variational wave function, we show that the entanglement enhancement is present not only at $\nu=1/2$ but also at $\nu=1/4$, as well as in bosonic CFL states at $\nu=1$ and $\nu=1/3$ fillings. In all cases, we find the scaling of S_2 with subsystem size to be enhanced compared to the non-interacting case, and insensitive to the choice of geometry and projection to the lowest Landau level. We also demonstrate that the variance of the particle number in a subsystem obeys area-law scaling with a universal subleading corner contribution, in stark contrast with free fermions. Our results establish the enhanced entanglement scaling and suppressed charge fluctuations as fingerprints of non-Fermi-liquid correlations in the CFL state.

Introduction.—The fundamental quasiparticles of fractional quantum Hall states are composite fermions (CFs) – electrons dressed by an even number of vortices of the magnetic flux [1]. At even-denominator fillings of the lowest Landau level (LLL), CFs can form a compressible state – the “composite fermion Fermi liquid” (CFL) [2–4], which has been observed in numerous experiments [5]. The CFL state has also been argued to emerge in systems with flat bands in the absence of a magnetic field, such as twisted moiré materials [6, 7].

Flux attachment – the mechanism behind the formation of CFs [2, 8, 9] – couples their Fermi surface with an internal statistical $U(1)$ gauge field, placing CFLs inside a larger class of “non-Fermi liquids” (NFLs) (see Ref. [10] for a recent review). On the one hand, the CFL is a pristine example of a stable NFL phase that emerges solely due to electron-electron interactions. On the other hand, the existence of well-defined quasiparticles implies there may be a good degree of qualitative similarity between CFL and conventional Fermi liquids [11–13]. Indeed, the Fermi wave vector of CFs is consistent with that derived from the electron density [14–16] and it also satisfies the Luttinger theorem [17, 18]. Thus, pinpointing the NFL nature of the CFL is a nontrivial task.

One sensitive diagnostic of any quantum state is its bipartite entanglement entropy. The entanglement entropy scaling in non-interacting Fermi liquids obeys the well-known Widom formula [19–21], wherein the “area law” – ubiquitous to gapped systems – gets modified by a multiplicative logarithmic correction. It has been ar-

gued that turning on interactions leads to the same scaling [22], leaving open the value of the prefactor [23, 24]. Previous numerical tests of this hypothesis for the CFL state have arrived at conflicting conclusions. Infinite density matrix renormalization group (iDMRG) study of the Coulomb ground state at $\nu=1/2$ revealed no sign of correction to the Widom formula [25]. For the continuum CFL variational wave function of Rezayi and Read [26], Ref. [27] found a significant multiplicative prefactor to the entanglement entropy scaling (≈ 2 in system sizes on the order of 40 electrons). Lastly, Ref. [28] also found an enhancement for a lattice analog of the CFL wave function. However, based on the scaling of different contributions to the entanglement from the sign and modulus of the wave function, Ref. [28] ruled out the enhancement as a finite-size effect. These studies therefore raise an important question: is there any distinctive entanglement signature of the CFL state in the thermodynamic limit?

Here we report a systematic study of entanglement in several spinless CFLs described by the Rezayi-Read continuum wave function [26]. We compare the fermionic CFLs at filling factors $\nu=1/2$ and $\nu=1/4$, which are distinguished by the number of vortices attached to each electron (two and four, respectively), and contrast those against an odd number of vortices in bosonic CFLs at $\nu=1$ and $\nu=1/3$ fillings. We employ Monte Carlo techniques to evaluate the second Rényi entropy using the SWAP algorithm [30]. In all CFL states considered, we find an enhancement of entanglement scaling, consistent with Ref. [27]. At the same time, we reconcile these find-

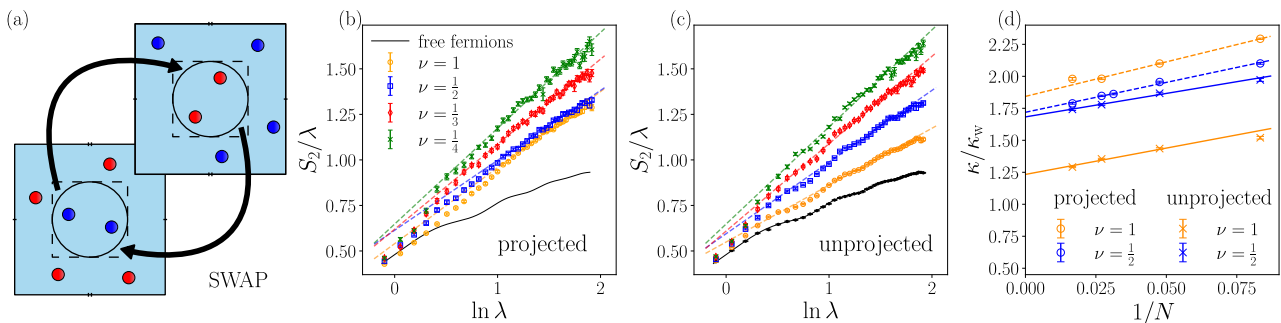


FIG. 1. (a): Illustration of the Monte Carlo SWAP algorithm: interchanging the highlighted regions of two copies of the system yields the second Rényi entropy S_2 . For entanglement calculations, we use circular subregions, while for charge fluctuations we use the square (dashed) subregion to capture the corner contributions. (b)-(c): S_2 of CFLs on the square torus for projected (b) and unprojected (c) wave functions at fillings $\nu=1/m$, with $m=1, 2, 3, 4$. For all fillings, S_2 exhibits a multiplicative correction ~ 1.7 to the Widom formula [Eq. (3)]. The $2k_F$ Friedel oscillations [2] are visible in all cases. All data is for $N=37$ particles. Crosses represent Monte Carlo data, while the continuous line is the exact diagonalization result for free fermions. (d) Extrapolations of the ratio between the slope κ (S_2 vs. $\lambda \ln \lambda$) of the CFL at fillings $\nu=1/2$ and $\nu=1$ and the free-fermion slope κ_w . We used system sizes $N=12-60$ and data points in the range which yield the extrapolated free-fermion slope ≈ 0.25 [29].

ings with entropy decompositions considered in Ref. [28] by showing that the latter is more sensitive to finite-size effects and LLL projection compared to the total entropy. We demonstrate the robustness of our conclusions in sphere and torus geometries. Finally, we use the same setup to evaluate charge fluctuations in a subsystem, for which analytical predictions are available [31]. We confirm that charge fluctuations in the CFL state follow the expected area-law scaling, in sharp contrast with free fermions. Moreover, within the same range of system sizes, we accurately extract the subleading corner contribution to the charge fluctuations, in agreement with the expected “super-universal” value [31] that also holds for gapped [32, 33] and critical states [34, 35] in $(2+1)$ -dimension.

CFL wave function.—The CFL state at filling factor $\nu=1/m$ is described by the ansatz wave function [26]:

$$\Psi_m^{\text{CFL}} = \text{Det}[\chi_n(z_j, z_j^*)] \prod_{i < j} (z_i - z_j)^m e^{-\frac{1}{4} \sum_k |z_k|^2}. \quad (1)$$

The first term is a Slater determinant of single-particle orbitals χ_n occupied by CFs in zero magnetic field, and the remainder is the Laughlin wave function at filling $\nu=1/m$ [36], expressed in terms of particle coordinates $z_j = x_j + iy_j$ with the magnetic length set to unity. Note that, due to the antisymmetry of the Slater determinant, these wave functions describe fermionic CFL states for m even and bosonic CFL states for m odd. The wave functions of Eq (1) can be adapted to the spherical and torus geometries considered in this work, see Refs. [26, 37, 38] and the Supplementary Material (SM) [29]. Moreover, the wave function of Eq. (1) is not constrained to reside in the LLL. To make contact with previous work, we will project the wave function to the LLL using the Jain-Kamilla method [27, 39–41]. Nevertheless, we will probe the sensitivity of our results by also considering

the unprojected wave function as written in Eq. (1).

Rényi entropy.—The object of our study is the second Rényi entropy of the reduced density matrix $\hat{\rho}_A$ of region A :

$$S_2 = -\ln(\text{tr}_A \hat{\rho}_A^2), \quad \hat{\rho}_A = \text{tr}_{\bar{A}} |\Psi_m^{\text{CFL}}\rangle \langle \Psi_m^{\text{CFL}}|, \quad (2)$$

obtained by tracing over the complement \bar{A} . In most of our calculations, we take A to be a circular subregion of radius r_A , see Fig. 1(a), although later we will also consider a square-shaped region to determine corner contributions to charge fluctuations in A . To extract the scaling, we fix a large system size and vary r_A . S_2 can be conveniently evaluated via variational Monte Carlo by replacing the trace with an expectation value of a SWAP operator between two copies of the system [30], which we review in the SM [29].

For free fermions in 2D, the area-law scaling of S_2 is violated by a term that depends logarithmically on the dimensionless quantity $\lambda \equiv k_F r_A$, with k_F denoting the Fermi momentum. The violation is given by the asymptotic Widom formula [19–21]:

$$S_2^{\text{free}} = \kappa_w \lambda \ln \lambda + \dots, \quad (3)$$

where κ_w is the Widom coefficient that depends solely on the geometry and effective central charge of a $(1+1)$ -dimensional chiral relativistic fermion [42, 43]. For a circular 2D Fermi surface, we have $\kappa_w=1/4$. One of the goals of this paper is to ascertain whether the entropy of CFL states follows the scaling $S_2 = \kappa \lambda \ln \lambda + \dots$, analogous to Eq. (3), and whether κ is the same as κ_w .

In Fig. 1 we show the evaluated S_2 for bosonic and fermionic CFL states at fillings $\nu=1/m$, with $m=1, 2, 3, 4$. Based on our free-fermion benchmarks, to minimize the finite-size effect, we harvest data points such that the subsystem area ranges from 1% to 30% of the total area,

and use a fixed Fermi momentum of $k_F = \sqrt{2\nu}$. Our results for $\nu=1/2$ are consistent with Ref. [27] and scaling in Eq. (3), with the coefficient $\kappa \approx 1.7\kappa_w$ violating the Widom formula. By comparing the circular and square subregions, we find the violation to be independent of the subregion shape [29]. Furthermore, attaching a different number of vortices only has a weak effect on the slope κ . Moreover, LLL projection also has an almost negligible effect on κ , except for the bosonic $\nu=1$ CFL state. The stronger effect of LLL projection on $\nu=1$ is expected based on the single vortex attached [29]. Finally, while Fig. 1 is for the torus geometry, we find a similar enhancement of entanglement scaling for CFL states on the sphere [29].

Charge fluctuations.—In systems with a U(1) symmetry, entanglement can be directly related to fluctuations of particle number, \hat{N}_A , in a subsystem:

$$\Delta^2 N_A \equiv \langle \hat{N}_A^2 \rangle - \langle \hat{N}_A \rangle^2. \quad (4)$$

For example, in non-interacting 2D Fermi liquids, S_2 and $\Delta^2 N_A$ differ only by a multiplicative constant [44, 45]. Similarly, in a NFL, charge fluctuations are expected to closely track entanglement entropy [46]. Recently, the scaling of charge cumulants or “disorder operators” was indeed shown to exhibit a logarithmic violation of the area law in NFLs at a quantum critical point [47]. Since $\Delta^2 N_A$ can be computed with a similar Monte Carlo method and system sizes as S_2 , we can leverage the better analytical understanding of charge fluctuations to support our previous entanglement results.

Remarkably, Fig. 2 shows that $\Delta^2 N_A$ in CFL states obeys an area law, irrespective of LLL projection and in stark contrast with ordinary Fermi liquids. The electrons in a CFL have been argued to exhibit an effective *finite* correlation length, leading to an exponentially suppressed tunneling density of states [48–51] and a Coulomb gap observed in experiment [52–56]. This implies that charge fluctuations of the physical electrons forming the CFL are *gapped* and should follow an area law [31, 57]. This striking property of the CFL state, to the best of our knowledge, has not previously been demonstrated for the CFL wave function.

In spatially isotropic systems, the behavior of $\Delta^2 N_A$ is governed by the static structure factor [33]. For CFL states, the LLL-projected structure factor takes the form $s_q \sim q^3 \ln(1/q)$ in the long-wavelength limit [2, 11], with inter-Landau level gapped modes contributing an additional term $\sim q^2$. The former enforces an area law scaling, while the latter adds a “super-universal” constant term in the presence of sharp corners, e.g., for the square subsystem in Fig. 1(a). The general form is

$$\Delta^2 N_A = a\lambda - b(\theta) + \dots, \quad b(\theta) = \frac{\nu}{4\pi^2}(1 + (\pi - \theta) \cot \theta), \quad (5)$$

where a is a non-universal coefficient, and $b(\theta)$ is a constant contribution due to a bipartition containing a single

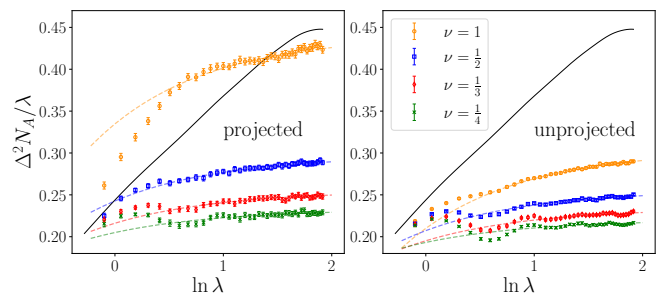


FIG. 2. Charge fluctuations across the bipartition for CFL states at different filling factors. In contrast to free fermions (solid black line), the charge fluctuations in CFL states are strongly suppressed and obey area-law scaling (plots on a linear λ scale are shown in SM [29] and the colored dashed lines represent fits to the area law). LLL projection alters the area law coefficient but preserves the universal corner contribution. Table I shows the extracted corner contributions, which are proportional to the filling.

corner with an opening angle θ [31]. From the intercept of $\Delta^2 N_A$ vs. λ , we determined $b(\pi/2)$ in Table I, which is in good agreement with Eq. (5). Note that while projection places the wave functions of Eq. (1) completely inside the LLL, we do not project the density operator, and therefore the associated gapped modes are not removed, hence both projected and unprojected wave functions exhibit approximately the same corner contribution.

	$\nu=1$	$\nu=1/2$	$\nu=1/3$	$\nu=1/4$
$4\pi^2 b_{\text{theory}}$	1	0.5	1/3	0.25
$4\pi^2 b_{\text{proj}}$	1.04(9)	0.53(4)	0.38(6)	0.28(6)
$4\pi^2 b_{\text{unproj}}$	0.93(3)	0.48(4)	0.39(4)	0.27(5)

TABLE I. Extracted corner contributions to charge fluctuations in different CFL states, with or without LLL projection. The system size is $N=37$ particles for all fillings.

Modulus and sign structure.—While Fig. 1 is strongly suggestive of κ exceeding the Widom value, it is important to understand where this enhancement is structurally encoded in a CFL wave function and whether or not it should be interpreted as a finite-size effect [28]. An idea first put forward in Ref. [58] in the context of gapped spin liquids, is to decompose the total entropy in a way inspired by SWAP:

$$S_2(\Psi) = S_2(|\Psi\rangle) + S_{2,\text{sign}}, \quad (6)$$

where $S_2(|\Psi\rangle)$ is the entropy of the absolute value of the wave function, while $S_{2,\text{sign}}$ stems from an interplay between the absolute value and the sign structure of Ψ [29].

The hope behind the decomposition of Eq. (6) is that the sign structure of the wave function carries the leading contribution to the entanglement as $N \rightarrow \infty$. While there are examples of sign wave functions with provable large entanglement [59, 60], the scaling of different terms

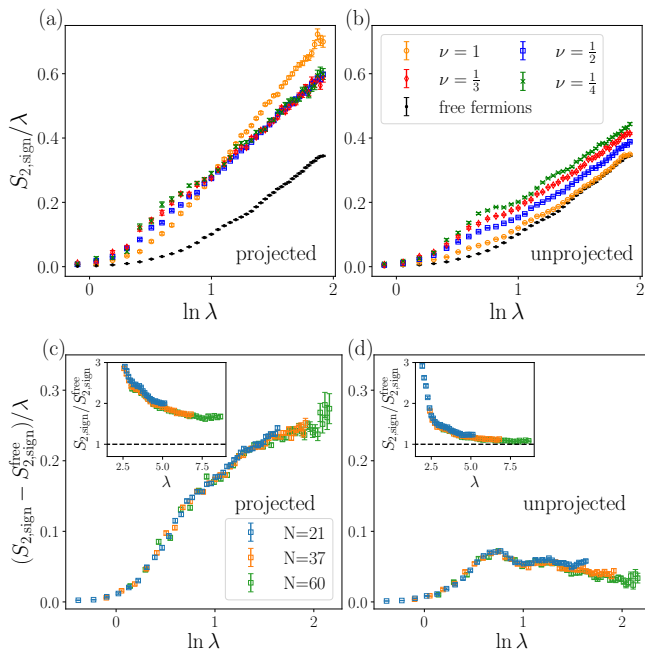


FIG. 3. Sign entropy for projected (a) and unprojected (b) CFL states for $N = 37$ particles on a torus. For comparison, we also show the result for free fermions, with the same data plotted in (a) and (b). Unprojected CFL states appear to behave similarly to free fermions, while projected wave functions show an enhanced slope. This is revealed by plotting the difference of $S_{2,\text{sign}}$ for the $\nu=1/2$ CFL relative to free fermions in panels (c)-(d): the difference grows in the projected case (c), while it decays towards zero in the unprojected case (d). Insets in (c)-(d) show the ratio of CFL sign entropy to that of free fermions, which shows qualitatively similar behavior.

with N in Eq. (6) is not rigorously understood in general. Indeed, even for free fermions, the scaling of $S_2(|\Psi\rangle)$ and $S_{2,\text{sign}}$ are not known analytically. Our Monte Carlo analysis for free fermions in SM [29] is consistent with $S_{2,\text{sign}}$ carrying the dominant $\lambda \ln \lambda$ dependence, however both $S_2(|\Psi\rangle)$ and $S_{2,\text{sign}}$ suffer from much more pronounced finite-size effects compared to the total entropy S_2 . Consequently, the decomposition given in Eq. (6) obscures the interpretation of the data as it replaces a tractable free-fermion problem with an effectively “many-body” object that carries non-trivial finite-size dependence due to the mixing of subleading [$\mathcal{O}(\lambda)$ and $\mathcal{O}(\ln \lambda)$] terms.

Similar issues are observed in the sign entropy of projected and unprojected CFL states, shown in Fig. 3(a)-(b). Unlike the full entropy, which is largely insensitive to LLL projection, the sign entropies are significantly altered by it, although they still appear to capture the logarithmic violation of the area law. In particular, $S_{2,\text{sign}}$ of the unprojected CFL states tracks the sign entropy of free fermions, which is revealed more clearly by plotting their difference in Fig. 3(d), while the ratio is shown in the inset. By contrast, within the same range of system sizes, the difference $S_{2,\text{sign}} - S_{2,\text{sign}}^{\text{free}}$ increases with λ for

the projected CFL states in Fig. 3(c), consistent with an enhancement.

As the physical content and scaling properties of the sign entropy are unclear, one should not view the results in Fig. 3 as more compelling than the full entropy in Fig. 1. Nevertheless, if one assumes that $S_{2,\text{sign}}$ may carry the leading $\lambda \ln \lambda$ dependence, it is interesting to ponder two scenarios that would make Figs. 1 and 3 consistent. The first possibility is that there may be an intrinsic difference between projected and unprojected CFL states, such that only the former exhibits an enhanced entanglement growth. While this is counterintuitive, LLL projection could alter the coefficient of entanglement scaling, unlike other universal topological properties. The second option, proposed by Ref. [28], is to conclude there is no enhancement and place trust in Figs. 3(b)-(d) above all others. This would require the lines in Figs. 3(a)-(c) to ultimately undergo a downturn, with a corresponding reduction of slope in Fig. 1. Based on the existing data, we estimate that observing this would require system sizes $N \gtrsim 300$, which are significantly beyond current computational capability.

The similarity of our unprojected results in Fig. 3(b) with Ref. [28] is attributed to the lack of an explicit band projection in the lattice realization of the CFL state. By contrast, our LLL-projected results in Fig. 1 show a visible departure from Ref. [28], e.g., the entropy of the bosonic $\nu=1$ CFL is similar to that of the fermionic $\nu=1/2$ CFL state after LLL projection, unlike their lattice analogs in Ref. [28]. These differences point to a subtle role of LLL projection, precluding direct comparisons between continuum and lattice versions of the CFL state, and potentially implying that entanglement scaling may depend on the microscopic details of flux attachment. A related question is whether the Chern band projection has a similar effect on the entanglement of CFL in zero magnetic field [6, 7], or whether the latter also depends on band geometry and Chern number.

Discussion.—We have evaluated the scaling of S_2 Rényi entropy of CFL states at different fillings $\nu=1/m$ and showed that it obeys the Widom scaling as in ordinary Fermi liquids but with an enhanced prefactor. We have found an enhancement in both the sphere and torus geometry; moreover, for $m \geq 2$, the enhancement is essentially unaffected by the LLL projection. We corroborated these conclusions by demonstrating that the wave function [Eq. (1)] encodes the expected area law for charge fluctuations with a universal corner contribution.

Our results for $m=2$ are in agreement with Ref. [27], while the discrepancy with Ref. [28] is, at least partly, due to the LLL projection which was not explicitly enforced on the lattice. Moreover, we pointed out the difficulties of interpreting the entropy scalings of the modulus and sign parts of the wave function, arguing that the total entropy is a more robust quantity in the range of numerically accessible system sizes.

One remaining enigma is how to reconcile our results with the iDMRG study of the $\nu=1/2$ CFL state on an infinite cylinder, where no enhancement to the Widom formula was found [25]. Two important differences in the setup of Ref. [25] are the quasi-1D geometry, which can impact the behavior of the 2D structure factor [61], and the study of the ground state of the Coulomb interaction rather than a variational wave function. Properties of the CFL for long-range interactions are known to be more similar to those of an ordinary Fermi liquid, while the differences are amplified by shorter-range interactions [2]. While our wave function [Eq. (1)] is not an exact ground state of any known Hamiltonian, it would be interesting to repeat the analysis of Ref. [25] and check the impact of short-range interaction on κ . Ultimately, the enhanced entanglement scaling in CFL states should be understood analytically. We expect that further progress could be made using multi-dimensional bosonization [62, 63], or by finding other observables whose fluctuations violate the area law, as recently achieved for the gapless Mott insulator with a spinon Fermi surface [31, 47].

Acknowledgments.—We are grateful to Luca Delacrétaz, Benoit Estienne, Nicolas Regnault, Xiaochuan Wu, and Kun Yang for useful discussions, and to Ryan Mishmash for generously sharing his lattice Monte Carlo code with us and for helpful comments on our manuscript. We acknowledge support by the Leverhulme Trust Research Leadership Award RL-2019-015, Royal Society International Exchanges Grant IES\R2\202052 and the Science and Engineering Research Board (SERB) of the Department of Science and Technology (DST) for financial support through the Mathematical Research Impact Centric Support (MATRICS) Grant No. MTR/2023/000002. This research was supported in part by grants NSF PHY-1748958 and PHY-2309135 to the Kavli Institute for Theoretical Physics (KITP). Computational portions of this research work were carried out on ARC3 and ARC4, part of the High-Performance Computing facilities at the University of Leeds, UK.

* z.papic@leeds.ac.uk

- [1] J. K. Jain, Composite-fermion approach for the fractional quantum Hall effect, *Phys. Rev. Lett.* **63**, 199 (1989).
- [2] B. I. Halperin, P. A. Lee, and N. Read, Theory of the half-filled Landau level, *Phys. Rev. B* **47**, 7312 (1993).
- [3] V. Pasquier and F. Haldane, A dipole interpretation of the $\nu = 1/2$ state, *Nuclear Physics B* **516**, 719 (1998).
- [4] N. Read, Lowest-Landau-level theory of the quantum Hall effect: The Fermi-liquid-like state of bosons at filling factor one, *Phys. Rev. B* **58**, 16262 (1998).
- [5] M. Shayegan, Probing composite fermions near half-filled Landau levels, in *Fractional Quantum Hall Effects: New Developments*, edited by B. I. Halperin and J. K. Jain (World Scientific Pub Co Inc, Singapore, 2020) Chap. 3, pp. 133–181.
- [6] J. Dong, J. Wang, P. J. Ledwith, A. Vishwanath, and D. E. Parker, Composite Fermi Liquid at Zero Magnetic Field in Twisted MoTe₂, *Phys. Rev. Lett.* **131**, 136502 (2023).
- [7] H. Goldman, A. P. Reddy, N. Paul, and L. Fu, Zero-Field Composite Fermi Liquid in Twisted Semiconductor Bilayers, *Phys. Rev. Lett.* **131**, 136501 (2023).
- [8] A. Lopez and E. Fradkin, Fractional quantum Hall effect and Chern-Simons gauge theories, *Phys. Rev. B* **44**, 5246 (1991).
- [9] J. K. Jain, *Composite Fermions* (Cambridge University Press, New York, US, 2007).
- [10] D. Chowdhury, A. Georges, O. Parcollet, and S. Sachdev, Sachdev-Ye-Kitaev models and beyond: Window into non-Fermi liquids, *Rev. Mod. Phys.* **94**, 035004 (2022).
- [11] D. T. Son, Is the Composite Fermion a Dirac Particle?, *Phys. Rev. X* **5**, 031027 (2015).
- [12] C. Wang and T. Senthil, Composite Fermi liquids in the lowest Landau level, *Phys. Rev. B* **94**, 245107 (2016).
- [13] B. I. Halperin, The Half-Full Landau Level, in *Fractional Quantum Hall Effects: New Developments*, edited by B. I. Halperin and J. K. Jain (World Scientific Pub Co Inc, Singapore, 2020) Chap. 2, pp. 79–132.
- [14] D. Kamburov, Y. Liu, M. A. Mueed, M. Shayegan, L. N. Pfeiffer, K. W. West, and K. W. Baldwin, What Determines the Fermi Wave Vector of Composite Fermions?, *Phys. Rev. Lett.* **113**, 196801 (2014).
- [15] D. Kamburov, M. A. Mueed, I. Jo, Y. Liu, M. Shayegan, L. N. Pfeiffer, K. W. West, K. W. Baldwin, J. J. D. Lee, and R. Winkler, Determination of Fermi contour and spin polarization of $\nu = \frac{3}{2}$ composite fermions via ballistic commensurability measurements, *Phys. Rev. B* **90**, 235108 (2014).
- [16] M. A. Mueed, D. Kamburov, S. Hasdemir, M. Shayegan, L. N. Pfeiffer, K. W. West, and K. W. Baldwin, Geometric resonance of composite fermions near the $\nu = 1/2$ fractional quantum Hall state, *Phys. Rev. Lett.* **114**, 236406 (2015).
- [17] A. C. Balram, C. Tóke, A. Wójs, and J. K. Jain, Spontaneous polarization of composite fermions in the $n = 1$ Landau level of graphene, *Phys. Rev. B* **92**, 205120 (2015).
- [18] A. C. Balram and J. K. Jain, Fermi wave vector for the partially spin-polarized composite-fermion Fermi sea, *Phys. Rev. B* **96**, 235102 (2017).
- [19] H. Widom, Operator theory: Adv, in *Appl*, Vol. 4 (1982) p. 477.
- [20] D. Gioev and I. Klich, Entanglement Entropy of Fermions in Any Dimension and the Widom Conjecture, *Phys. Rev. Lett.* **96**, 100503 (2006).
- [21] H. Leschke, A. V. Sobolev, and W. Spitzer, Scaling of Rényi Entanglement Entropies of the Free Fermi-Gas Ground State: A Rigorous Proof, *Phys. Rev. Lett.* **112**, 160403 (2014).
- [22] B. Swingle and T. Senthil, Universal crossovers between entanglement entropy and thermal entropy, *Phys. Rev. B* **87**, 045123 (2013).
- [23] J. McMinis and N. M. Tubman, Renyi entropy of the interacting Fermi liquid, *Phys. Rev. B* **87**, 081108 (2013).
- [24] W.-J. Hu, Y. Zhang, A. H. Nevidomskyy, E. Dagotto, Q. Si, and H.-H. Lai, Fractionalized excitations revealed by entanglement entropy, *Phys. Rev. Lett.* **124**, 237201 (2020).
- [25] S. D. Geraedts, M. P. Zaletel, R. S. K. Mong, M. A. Metl-

- itski, A. Vishwanath, and O. I. Motrunich, The half-filled Landau level: The case for Dirac composite fermions, *Science* **352**, 197 (2016).
- [26] E. Rezayi and N. Read, Fermi-liquid-like state in a half-filled Landau level, *Phys. Rev. Lett.* **72**, 900 (1994).
- [27] J. Shao, E.-A. Kim, F. D. M. Haldane, and E. H. Rezayi, Entanglement Entropy of the $\nu = 1/2$ Composite Fermion Non-Fermi Liquid State, *Phys. Rev. Lett.* **114**, 206402 (2015).
- [28] R. V. Mishmash and O. I. Motrunich, Entanglement entropy of composite Fermi liquid states on the lattice: In support of the Widom formula, *Phys. Rev. B* **94**, 081110 (2016).
- [29] See the Supplemental Material for detailed information about the calculations and results in the main text.
- [30] M. B. Hastings, I. González, A. B. Kallin, and R. G. Melko, Measuring Renyi entanglement entropy in quantum Monte Carlo simulations, *Phys. Rev. Lett.* **104**, 157201 (2010).
- [31] X.-C. Wu, Bipartite fluctuations of critical Fermi surfaces (2024), [arXiv:2404.04331 \[cond-mat.str-el\]](https://arxiv.org/abs/2404.04331).
- [32] B. Estienne, J.-M. Stéphan, and W. Witczak-Krempa, Cornering the universal shape of fluctuations, *Nature Communications* **13**, 287 (2022).
- [33] C. Berthiere, B. Estienne, J.-M. Stéphan, and W. Witczak-Krempa, Full-counting statistics of corner charge fluctuations, *Phys. Rev. B* **108**, L201109 (2023).
- [34] X.-C. Wu, C.-M. Jian, and C. Xu, Universal features of higher-form symmetries at phase transitions, *SciPost Phys.* **11**, 033 (2021).
- [35] Y.-C. Wang, M. Cheng, and Z. Y. Meng, Scaling of the disorder operator at $(2 + 1)d$ U(1) quantum criticality, *Phys. Rev. B* **104**, L081109 (2021).
- [36] R. B. Laughlin, Anomalous Quantum Hall Effect: An Incompressible Quantum Fluid with Fractionally Charged Excitations, *Phys. Rev. Lett.* **50**, 1395 (1983).
- [37] M. Fremling, N. Moran, J. K. Slingerland, and S. H. Simon, Trial wave functions for a composite Fermi liquid on a torus, *Phys. Rev. B* **97**, 035149 (2018).
- [38] S. D. Geraedts, J. Wang, E. H. Rezayi, and F. D. M. Haldane, Berry phase and model wave function in the half-filled Landau level, *Phys. Rev. Lett.* **121**, 147202 (2018).
- [39] J. K. Jain and R. K. Kamilla, Composite fermions in the Hilbert space of the lowest electronic Landau level, *Int. J. Mod. Phys. B* **11**, 2621 (1997).
- [40] S. Pu, Y.-H. Wu, and J. K. Jain, Composite fermions on a torus, *Phys. Rev. B* **96**, 195302 (2017).
- [41] S. Pu, M. Fremling, and J. K. Jain, Berry phase of the composite-fermion Fermi sea: Effect of Landau-level mixing, *Phys. Rev. B* **98**, 075304 (2018).
- [42] B. Swingle, Entanglement Entropy and the Fermi Surface, *Phys. Rev. Lett.* **105**, 050502 (2010).
- [43] B. Swingle, Conformal field theory approach to Fermi liquids and other highly entangled states, *Phys. Rev. B* **86**, 035116 (2012).
- [44] P. Calabrese, M. Mintchev, and E. Vicari, Entanglement entropies in free-fermion gases for arbitrary dimension, *Europhysics Letters* **97**, 20009 (2012).
- [45] M. T. Tan and S. Ryu, Particle number fluctuations, Rényi entropy, and symmetry-resolved entanglement entropy in a two-dimensional Fermi gas from multidimensional bosonization, *Phys. Rev. B* **101**, 235169 (2020).
- [46] B. Swingle and T. Senthil, Universal crossovers between entanglement entropy and thermal entropy, *Phys. Rev. B* **87**, 045123 (2013).
- [47] W. Jiang, B.-B. Chen, Z. H. Liu, J. Rong, F. F. Asaad, M. Cheng, K. Sun, and Z. Y. Meng, Many versus one: The disorder operator and entanglement entropy in fermionic quantum matter, *SciPost Phys.* **15**, 082 (2023).
- [48] M. Barkeshli, M. Mulligan, and M. P. A. Fisher, Particle-hole symmetry and the composite Fermi liquid, *Phys. Rev. B* **92**, 165125 (2015).
- [49] S. He, S. Das Sarma, and X. C. Xie, Quantized Hall effect and quantum phase transitions in coupled two-layer electron systems, *Phys. Rev. B* **47**, 4394 (1993).
- [50] Y. B. Kim and X.-G. Wen, Instantons and the spectral function of electrons in the half-filled Landau level, *Phys. Rev. B* **50**, 8078 (1994).
- [51] S. Pu, A. C. Balram, Y. Hu, Y.-C. Tsui, M. He, N. Regnault, M. P. Zaletel, A. Yazdani, and Z. Papić, Fingerprints of Composite Fermion Lambda Levels in Scanning Tunneling Microscopy (2023), [arXiv:2312.06779 \[cond-mat.mes-hall\]](https://arxiv.org/abs/2312.06779).
- [52] R. C. Ashoori, J. A. Lebens, N. P. Bigelow, and R. H. Silsbee, Equilibrium tunneling from the two-dimensional electron gas in GaAs: Evidence for a magnetic-field-induced energy gap, *Phys. Rev. Lett.* **64**, 681 (1990).
- [53] J. P. Eisenstein, L. N. Pfeiffer, and K. W. West, Coulomb barrier to tunneling between parallel two-dimensional electron systems, *Phys. Rev. Lett.* **69**, 3804 (1992).
- [54] X. Liu, G. Farahi, C.-L. Chiu, Z. Papić, K. Watanabe, T. Taniguchi, M. P. Zaletel, and A. Yazdani, Visualizing broken symmetry and topological defects in a quantum Hall ferromagnet, *Science* **375**, 321 (2022).
- [55] G. Farahi, C.-L. Chiu, X. Liu, Z. Papić, K. Watanabe, T. Taniguchi, M. P. Zaletel, and A. Yazdani, Broken symmetries and excitation spectra of interacting electrons in partially filled Landau levels, *Nature Physics* **10.1038/s41567-023-02126-z** (2023).
- [56] Y. Hu, Y.-C. Tsui, M. He, U. Kamber, T. Wang, A. S. Mohammadi, K. Watanabe, T. Taniguchi, Z. Papić, M. P. Zaletel, and A. Yazdani, High-resolution tunneling spectroscopy of fractional quantum Hall states (2023), [arXiv:2308.05789 \[cond-mat.mes-hall\]](https://arxiv.org/abs/2308.05789).
- [57] K.-L. Cai and M. Cheng, Disorder operators in 2D Fermi and non-Fermi liquids through multidimensional bosonization (2024), [arXiv:2404.04334 \[cond-mat.str-el\]](https://arxiv.org/abs/2404.04334).
- [58] Y. Zhang, T. Grover, and A. Vishwanath, Entanglement Entropy of Critical Spin Liquids, *Phys. Rev. Lett.* **107**, 067202 (2011).
- [59] T. Grover and M. P. A. Fisher, Quantum disentangled liquids, *Journal of Statistical Mechanics: Theory and Experiment* **2014**, P10010 (2014).
- [60] N. Kaplis, F. Krüger, and J. Zaanen, Entanglement entropies and fermion signs of critical metals, *Phys. Rev. B* **95**, 155102 (2017).
- [61] P. Kumar and F. D. M. Haldane, Neutral excitations of quantum Hall states: A density matrix renormalization group study, *Phys. Rev. B* **106**, 075116 (2022).
- [62] W. Ding, A. Seidel, and K. Yang, Entanglement Entropy of Fermi Liquids via Multidimensional Bosonization, *Phys. Rev. X* **2**, 011012 (2012).
- [63] K.-L. Cai and M. Cheng, Disorder operators in 2d fermi and non-fermi liquids through multidimensional bosonization (2024), [arXiv:2404.04334 \[cond-mat.str-el\]](https://arxiv.org/abs/2404.04334).
- [64] F. D. M. Haldane and E. H. Rezayi, Periodic Laughlin-Jastrow wave functions for the fractional quantized Hall

- effect, *Phys. Rev. B* **31**, 2529 (1985).
- [65] F. D. M. Haldane, Many-particle translational symmetries of two-dimensional electrons at rational Landau-level filling, *Phys. Rev. Lett.* **55**, 2095 (1985).
- [66] S. Pu, Hall viscosity of the composite-fermion Fermi seas for fermions and bosons, *Phys. Rev. B* **102**, 165101 (2020).
- [67] S. Pu, M. Fremling, and J. K. Jain, Hall viscosity of composite fermions, *Phys. Rev. Research* **2**, 013139 (2020).
- [68] F. D. M. Haldane, Fractional quantization of the Hall effect: A hierarchy of incompressible quantum fluid states, *Phys. Rev. Lett.* **51**, 605 (1983).
- [69] C.-C. Chang, N. Regnault, T. Jolicoeur, and J. K. Jain, Composite fermionization of bosons in rapidly rotating atomic traps, *Phys. Rev. A* **72**, 013611 (2005).
- [70] Z. Liu, A. C. Balram, Z. Papić, and A. Gromov, Quench dynamics of collective modes in fractional quantum Hall bilayers, *Phys. Rev. Lett.* **126**, 076604 (2021).
- [71] A. C. Balram, C. Töke, A. Wójs, and J. K. Jain, Fractional quantum Hall effect in graphene: Quantitative comparison between theory and experiment, *Phys. Rev. B* **92**, 075410 (2015).
- [72] A. C. Balram and J. K. Jain, Nature of composite fermions and the role of particle-hole symmetry: A microscopic account, *Phys. Rev. B* **93**, 235152 (2016).
- [73] M.-C. Chung and I. Peschel, Density-matrix spectra of solvable fermionic systems, *Phys. Rev. B* **64**, 064412 (2001).
- [74] I. Klich, Lower entropy bounds and particle number fluctuations in a Fermi sea, *Journal of Physics A: Mathematical and General* **39**, L85 (2006).
- [75] P. Calabrese, M. Mintchev, and E. Vicari, Entanglement Entropy of One-Dimensional Gases, *Phys. Rev. Lett.* **107**, 020601 (2011).
- [76] A. Lukin, M. Rispoli, R. Schittko, M. E. Tai, A. M. Kaufman, S. Choi, V. Khemani, J. Léonard, and M. Greiner, Probing entanglement in a many-body-localized system, *Science* **364**, 256 (2019).
- [77] Ryan Mishmash, private communication.

Supplemental Online Material for “Enhanced entanglement scaling and area-law charge fluctuationn a non-Fermi liquid of composite fermions”

This Supplemental Material contains (i) expressions for CFL wave functions on the sphere and torus; (ii) an overview of the Jain-Kamilla projection scheme, showing that our results are insensitive to the details of the projection scheme; (iii) analysis of the entanglement scaling and demonstration that the Widom violation is independent of the shape of the subregion; (iv) derivation of the free-fermion Widom formula on the sphere; (v) brief introduction to the SWAP algorithm and our implementation; (vi) analysis of the second Rényi entropy decomposition and charge fluctuations, along with the extraction of their scaling and corner contributions, respectively; (vii) entanglement entropy scaling for flux-attached CFL wave functions.

JAIN-KAMILLA PROJECTION FOR THE CFL WAVE FUNCTIONS ON THE SPHERE AND TORUS

In the main text, we have written down the CFL wave function in the infinite disk geometry. For numerical studies of the bulk properties of this wave function, it is more convenient to use compact geometries such as the sphere or torus. Here we explain how the wave functions from the main text can be adapted to such geometries. Since these wave functions do not fully reside in the lowest Landau level, we also briefly describe how the Jain-Kamilla (JK) projection is performed in the two geometries.

Torus

On the torus, the single-particle orbitals are plane waves, $\chi_n(\mathbf{r}_j) = \exp(i\mathbf{k}_n \cdot \mathbf{r}_j)$, with \mathbf{k}_n the wave vectors of the occupied states of the Fermi sea. The latter can be determined from an empirical rule given in Ref. [27, 37, 38]. The Laughlin wave function ψ_m^L is expressed in terms of Jacobi ϑ functions that depend on complex electron coordinates $z_j = x_j + iy_j$ and modular parameter τ of the torus [64]:

$$\psi_m^L = \vartheta \left[\frac{\frac{N-1}{2}}{m \frac{(N-1)}{2}} \right] \left(\frac{m \sum z_i}{L_1} \middle| m\tau \right) \prod_{i < j} \left\{ \vartheta \left[\frac{\frac{1}{2}}{\frac{1}{2}} \right] \left(\frac{z_i - z_j}{L_1} \middle| \tau \right) \right\}^m \exp \left(\sum_i \frac{z_i^2 - |z_i|^2}{4\ell^2} \right),$$

with ℓ being the magnetic length. We have implicitly chosen the zero momentum sector for the center-of-mass, and strictly periodic conditions for the torus [65]. Here, JK projection can be implemented according to Ref. [66], leading to the following family of projected wave functions:

$$\Psi_m^{\text{CFL,proj}[\boldsymbol{\alpha}]} = \vartheta \left[\frac{\frac{N-1}{2}}{m \frac{(N-1)}{2}} \right] \left(\frac{m \left(\sum z_i + i\ell^2 \sum k_i \right)}{L_1} \middle| m\tau \right) \text{Det}[g_{nl}^{[\boldsymbol{\alpha}]}] \exp \left(\sum_i \frac{z_i^2 - |z_i|^2}{4\ell^2} \right),$$

$$g_{nl}^{[\boldsymbol{\alpha}]} = e^{k_n(k_n + 2\bar{k}_n)\ell^2/4} e^{i(k_n + \bar{k}_n)z_l/2} \prod_{p=1}^{m/2} \prod_{j \neq l} \vartheta \left[\frac{\frac{1}{2}}{\frac{1}{2}} \right] \left(\frac{z_l + i\alpha_p k_n \ell^2 - z_j}{L_1} \middle| \tau \right),$$

where $g_{nl}^{\boldsymbol{\alpha}}$ are CF “single-particle” wave functions that now depend on all other coordinates and $\boldsymbol{\alpha} = (\alpha_1, \dots, \alpha_{m/2})$ are the JK projection coefficients. Torus periodicity enforces the constraint $\sum_{p=1}^{m/2} \alpha_p = m$. Note that, essentially, the LLL projection shifts the attached vortices by an amount proportional to the wavevector of the CF. This scheme encompasses all fermionic wave functions with even m ; for bosons, one needs to attach one additional set of Jastrows outside the wave function for $m \geq 3$ and remove one for $m = 1$.

To verify the consistency of our results for different choices of $\boldsymbol{\alpha}$, Fig. S1 shows the S_2 Rényi entropy scaling is nearly unchanged for two choices $\boldsymbol{\alpha} = (2, 2)$ and $\boldsymbol{\alpha} = (4, 0)$ at $\nu = 1/4$. Moreover, even the individual contributions to the entropy, $S_{2,p}$, $S_{2,\text{mod}}$ and $S_{2,\text{sign}}$, discussed below, are essentially the same for the two $\boldsymbol{\alpha}$ choices. This shows that S_2 Rényi entropy is insensitive to the details of JK projection coefficients, unlike some other quantities such as the Hall viscosity in Ref. [67].

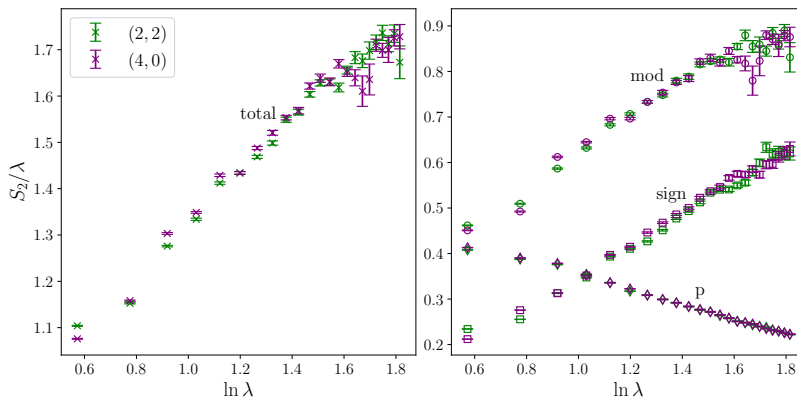


FIG. S1. The S_2 Rényi entropy (left panel) and its decomposition (right panel) for the two choices of JK projection coefficients, $\alpha = (2, 2)$ and $\alpha = (4, 0)$, at filling factor $\nu = 1/4$. The differences are seen to be minimal, the slope in particular agrees within the error bars, suggesting that details of the JK projection scheme are unimportant in determining the entanglement scaling. All data is for the system size of $N = 37$ electrons on the torus.

Sphere

On the sphere, the single-particle orbitals are the standard spherical harmonics, $\chi_n(\mathbf{r}_j) = Y_{L_n}^{M_n}(\theta_j, \varphi_j)$, where L , M stand for the angular momentum and its z -component, respectively, while θ_j , φ_j are the standard spherical angles describing the position of j th particle. The Laughlin wave function,

$$\psi_m^L = \prod_{i < j} (u_i v_j - v_i u_j)^m, \quad (\text{S1})$$

is expressed in terms of spherical spinor coordinates, $u_j = \sin(\theta_j/2) \exp(i\phi_j/2)$ and $v_j = \cos(\theta_j/2) \exp(-i\phi_j/2)$ [68]. Thus, the unprojected CFL wave function on the sphere has a very similar form to that written in the main text for the infinite plane. Fig. S2 demonstrates the similarity of unprojected CFL results on the sphere with those presented in the main text for the torus geometry. This consistency shows the robustness of our results, e.g., for the sequence of system sizes $N = n^2$ we consider on the sphere, the CFL has a uniform $L=0$ state, which removes some of the ambiguity associated with the definition of the Fermi momentum on the torus.

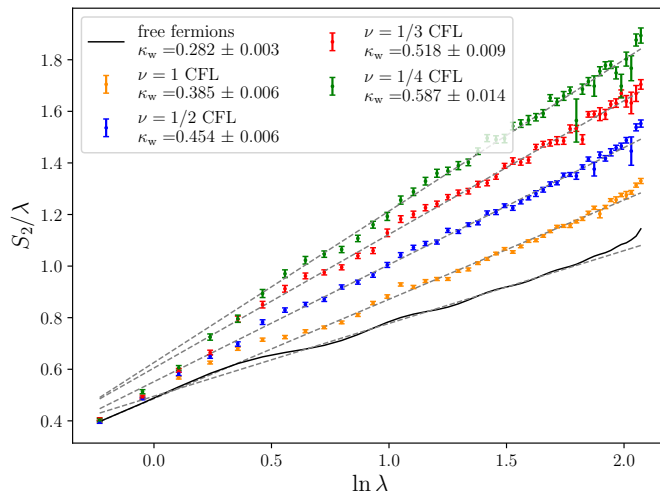


FIG. S2. Second Rényi entropy of unprojected CFL states on the sphere at fillings $\nu=1/m$, with $m=1, 2, 3, 4$. All data is for system size $N=64$. Crosses represent Monte Carlo data, while the continuous line for free fermions represents ED data. All filling factors show an enhanced slope compared to the Widom value.

Finally, we explain how to perform the projection on the sphere. Let us first treat the state at $\nu=1/2$, with

two vortices attached i.e., $\Psi_{1/2}^{\text{CFL}} = \mathcal{P}_{\text{LLL}} \prod_{j < k} (u_j v_k - u_k v_j)^2 \Phi_{\text{FS}}$, where Φ_{FS} is the filled-shell wave function on the sphere at zero-field that is analogous to that of a Fermi sea [26]. The projected state can be evaluated as a Slater determinant of CF wave functions, which now depend on the coordinates of all particles through the Jastrow factors $J_j = \prod_{k \neq j} (u_j v_k - u_k v_j)$. We quote the final expression here:

$$Y_{0LM}^{CF}(\Omega_j) = N_{0,L,M} (-1)^{L-M} \frac{(2Q+1)!}{(2Q+L+1)!} u_j^M v_j^{-M} \sum_{s=0}^L (-1)^s \binom{L}{s} \binom{L}{L-M-s} u_j^s v_j^{L-s} \left[\left(\frac{\partial}{\partial u_j} \right)^s \left(\frac{\partial}{\partial v_j} \right)^{L-s} J_j \right], \quad (\text{S2})$$

where $N_{0,L,M}$ is a normalization factor, and the flux for the physical electrons is $2Q=2(N-1)$. Given that we only have one power of Jastrow, the derivatives can be evaluated as follows:

$$\left(\frac{\partial}{\partial u_j} \right)^s \left(\frac{\partial}{\partial v_j} \right)^{L-s} J_j = J_j \sum_{i=0}^s \prod_{i=0}^s \frac{v_{k_i}}{u_j v_{k_i} - u_{k_i} v_j} \prod_{i=0}^{L-s} \frac{-u_{l_i}}{u_j v_{l_i} - u_{l_i} v_j}, \quad (\text{S3})$$

where the sum runs over all possibilities in choosing s particles $\{k_i\}$ and $L-s$ particles $\{l_i\}$, all distinct. The complete Jastrow factor J_i can be factored out of the determinant post-projection.

Note that the previous wave function directly allows construction for CFL states at different fillings. For the fermionic state at $\nu=1/4$, we choose to only project with two Jastrow factors, leaving the other two outside – this is similar to the $\alpha = (4, 0)$ state on the torus. For the bosonic states at $\nu=1$ and $\nu=1/3$, we need to divide or multiply by a single Jastrow factor respectively [69, 70], again mirroring the construction on the torus. It is known that the microscopic CFL wave function is not very sensitive to the number of Jastrows placed inside the LLL-projection operator [71, 72].

SHOPE EXTRAPOLATION AND SHAPE DEPENDENCE OF THE ENTANGLEMENT SCALING

Here we present additional data on the slope extrapolations used in Fig. 1(d) of the main text. Fig. S3(a) shows the data points used at system sizes $N \in \{12, 21, 32, 37, 60\}$ for the projected CFL wave function at $\nu=1/2$. We fix the smallest value to $\ln \lambda \approx 0.5$ regardless of system size, while the end point increases with N such that $\ln \lambda_{\text{end}} \in \{1.33, 1.51, 1.59, 1.66, 1.75\}$. These values are chosen to maximize the range of data points used at each system size, while still correctly extrapolating the correct Widom coefficient in the thermodynamic limit (see inset).

Fig. S3(b) and (c) show a comparison between systems with subregions of circular and square shape, respectively. We find the ratio of the slopes to be approximately independent of the subregion geometry. This indicates that the CFL entanglement scaling still encodes the geometric information in the Widom formula, with the violation limited to a numerical overall prefactor.

FREE FERMIONS

If a wave function Ψ can be written as a Slater determinant, $\Psi = \text{Det}[\phi_m(\mathbf{r}_n)]$, where the single-particle orbitals ϕ_m are orthonormalized over the full space, one can efficiently compute the entanglement entropy using the correlation matrix [73]. The correlation matrix \mathcal{A} has matrix elements given by the overlap integrals on the subsystem, $\mathcal{A}_{mn} = \int_A d\mathbf{r} \phi_m^*(\mathbf{r}) \phi_n(\mathbf{r})$. Suppose the eigenvalues of \mathcal{A} are a_m , $m = 1, 2, \dots, N$; the 2nd Renyi entropy is given by [74, 75]

$$S_2 = - \sum_m \ln (a_m^2 + (1 - a_m)^2). \quad (\text{S4})$$

In the torus geometry with a circular subregion A , the overlap matrix elements evaluate to:

$$\mathcal{A}_{mn}^{\text{torus}} = \int_A d\mathbf{r} \phi_m^*(\mathbf{r}) \phi_n(\mathbf{r}) = \frac{1}{L^2} \int_A d\mathbf{r} e^{i(\mathbf{k}_n - \mathbf{k}_m) \cdot \mathbf{r}} = \frac{2\pi}{L^2} \frac{r_A}{|\mathbf{k}_n - \mathbf{k}_m|} J_1(|\mathbf{k}_n - \mathbf{k}_m| r_A), \quad (\text{S5})$$

where J_1 is the Bessel function of the first kind. On the sphere, we obtain for a spherical cap subregion

$$\mathcal{A}_{mn}^{\text{sphere}} = \int_A d\Omega Y_{L_m M_m}^*(\Omega) Y_{L_n M_n}(\Omega) = 2\pi \mathcal{N}_{L_m M_m} \mathcal{N}_{L_n M_n} \delta_{M_m, M_n} \int_{\cos \theta_A}^1 dx P_{L_m}^{M_m}(x) P_{L_n}^{M_n}(x), \quad (\text{S6})$$

where $\mathcal{N}_{LM} = \sqrt{\frac{2L+1}{4\pi} \frac{(L+M)!}{(L-M)!}}$ is a normalization constant and the associated Legendre polynomial integrals can be computed recursively.

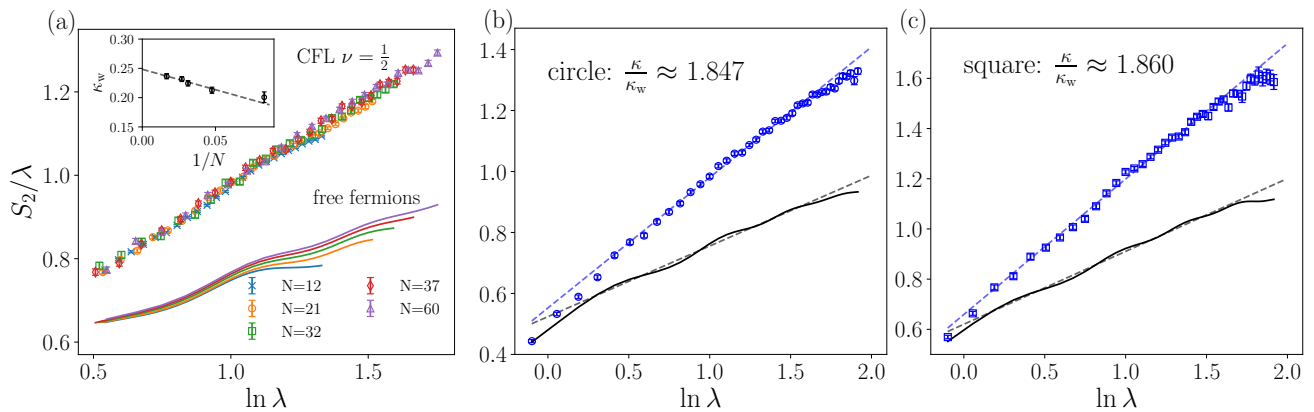


FIG. S3. Slope extrapolation and shape dependence of the entanglement scaling. (a): We extract the S_2 slope from a subset of data points in the λ -range shown here for various system sizes indicated in the legend. Solid lines are free-fermion data, while markers denote the projected CFL data at $\nu=1/2$. The range of λ values is chosen with free fermions as a benchmark, such that the correct Widom slope is recovered in the thermodynamic limit (inset). (b)-(c): The dependence of the entanglement scaling on the shape of the subregion, i.e., circle in (b) or square in (c). S_2 for free fermions (solid lines) and the projected CFL state at $\nu = 1/2$ (markers), for system size $N=37$. The ratio of slopes is the approximately independent of subregion geometry.

THE WIDOM FORMULA ON THE SPHERE

The intuitive derivation of the Widom formula given in Ref. [42] requires a few modifications in the spherical geometry. Suppose we have $N = n^2$ particles filling up n angular momentum shells. The $2n-1$ states of the last filled shell (the equivalent of the Fermi surface in the thermodynamic limit) are the ones that will contribute to the entanglement entropy. Therefore, one needs to replace the integral over the Fermi surface in the Widom formula,

$$\kappa_w^{(\alpha)} = \frac{c_{\text{eff}}(1+\alpha)}{12\alpha} \frac{1}{2} \int_{\partial\Omega} dS_x \int_{\partial\Gamma} dS_k \frac{|\hat{\mathbf{n}}_x \cdot \hat{\mathbf{n}}_k|}{2\pi}, \quad (\text{S7})$$

with a discrete sum over these modes. The flux factor $|\hat{\mathbf{n}}_x \cdot \hat{\mathbf{n}}_k|/2\pi$ needs to be replaced by $1/2\pi$, accounting for the rotational symmetry of the cap around the axis, and the double counting factor of $1/2$ becomes unnecessary. Then, the Renyi entropy for a spherical cap of angle θ is:

$$S_\alpha = \frac{c_{\text{eff}}(1+\alpha)}{12\alpha} \ln(R \sin \theta) \sum_{i=1}^{2n-1} \int_{\partial\Omega} \frac{dS_x}{2\pi} = \frac{c_{\text{eff}}(1+\alpha)}{12\alpha} (2\sqrt{N} - 1) \sin \theta \ln(R \sin \theta), \quad (\text{S8})$$

To enable a comparison between this and CFL states, we need to control the particle density through the flux. This, in turn, affects the definition of the radius R . For the CFL, the radius of the sphere is $R = \sqrt{Q}$ and the maximum occupied effective angular momentum is $L_{\text{max}} = \sqrt{N}$. Setting the radius of the cap to $R \sin \theta = \sqrt{Q} \sin \theta$, and the effective Fermi wave number $k_F = L_{\text{max}}/R = \sqrt{N/Q}$, we express the entropy in terms of the dimensionless length $\lambda_s = k_F \sqrt{Q} \sin \theta$:

$$S_2 = \left(\frac{1}{4} - \frac{1}{8\sqrt{N}} \right) \lambda_s \ln \lambda_s \approx \frac{1}{4} \lambda_s \ln \lambda_s, \quad (\text{S9})$$

in agreement with the torus in the large- N limit. Note that our derivation here does not capture finite-size effects related to the curvature of the sphere, which diminish in the limit $N \rightarrow \infty$.

CHARGE FLUCTUATIONS

In the main text, we presented the results for charge fluctuations in a subsystem, $\Delta^2 N_A$, normalized by λ and plotted as a function of $\ln \lambda$. This was done to show that charge fluctuations are clearly suppressed when plotted in the same way as the entanglement entropy, hence there is no logarithmic enhancement like in ordinary Fermi liquids, where charge fluctuations mirror the behavior of entanglement entropy. In Fig. S4 we show the same data for $\Delta^2 N_A$

but plotted on a linear λ scale, which shows the area law scaling of $\Delta^2 N_A$. From the linear fit to this data, we have extracted the intercept $\lambda \rightarrow 0$ in the insets of Fig. S4. This gives us the super-universal corner contribution, $4\pi^2 b(\pi/2)$, expected to approach ν [31–33].

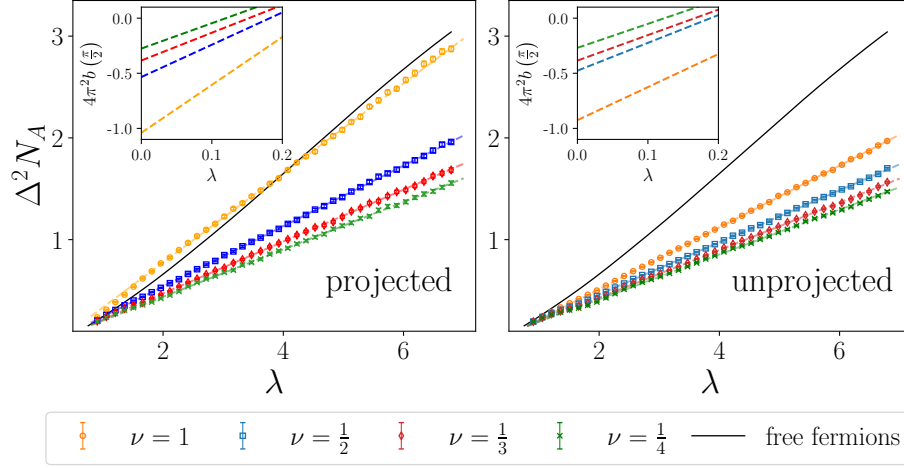


FIG. S4. Charge fluctuations across the bipartition for CFL states at different filling factors. In contrast to free fermions (solid black line), the charge fluctuations in CFL states are strongly suppressed and obey area-law scaling (fits to area-law are plotted as colored dashed lines). LLL projection alters the area law coefficient but preserves the universal corner contribution. Table I shows the extracted corner contributions, which are proportional to the filling.

SWAP ALGORITHM AND ENTROPY DECOMPOSITION

Following Refs. [30, 58], in our Monte Carlo evaluations of S_2 Rényi entropy we replace the partial trace with an expectation value $\langle \text{SWAP}_A \rangle$ of the SWAP operator between two copies of the system, as illustrated in Fig. S5. This expectation value can be naturally broken down into a product of three terms:

$$\langle \text{SWAP}_A \rangle = P_{\text{SWAP}} \langle \text{SWAP}_{\text{mod}} \rangle \langle \text{SWAP}_{\text{sign}} \rangle. \quad (\text{S10})$$

The first term, P_{SWAP} , represents the probability that the two copies are “swappable”, for which we must have the same number of particles $N_1 = N_2$:

$$P_{\text{SWAP}} = \frac{\int d\alpha d\beta |\Psi(\alpha_1, \beta_1)|^2 |\Psi(\alpha_2, \beta_2)|^2 \delta_{N_1, N_2}}{\int d\alpha d\beta |\Psi(\alpha_1, \beta_1)|^2 |\Psi(\alpha_2, \beta_2)|^2}, \quad (\text{S11})$$

where $\alpha = (\alpha_1, \alpha_2)$ and $\beta = (\beta_1, \beta_2)$ denote the sets of coordinates for the particles inside or outside the bipartition contour, respectively. The resulting entropy $S_{2,p}$ is the higher Rényi counterpart of the von Neumann number entropy [76], which can be generalized as $S_{\alpha,p} = \frac{1}{1-\alpha} \ln \sum_{N_A} p(N_A)^\alpha$, where $p(N_A)$ is the probability of having N_A particles in the defined subregion.

The following two terms in Eq. (S10) are the “mod” and “sign” contributions, which are evaluated only in the subspace of swappable copies ($N_1 = N_2$),

$$\langle \text{SWAP}_{\text{mod}} \rangle = \frac{\int d\alpha d\beta \delta_{N_1, N_2} |\psi(\alpha_1, \beta_1)|^2 |\psi(\alpha_2, \beta_2)|^2 \left| \frac{\psi(\alpha_2, \beta_1) \psi(\alpha_1, \beta_2)}{\psi(\alpha_1, \beta_1) \psi(\alpha_2, \beta_2)} \right|}{\int d\alpha d\beta \delta_{N_1, N_2} |\psi(\alpha_1, \beta_1)|^2 |\psi(\alpha_2, \beta_2)|^2}, \quad (\text{S12})$$

$$\langle \text{SWAP}_{\text{sign}} \rangle = \frac{\int d\alpha d\beta \delta_{N_1, N_2} |\psi(\alpha_2, \beta_1) \psi(\alpha_1, \beta_2) \psi(\alpha_1, \beta_1) \psi(\alpha_2, \beta_2)| e^{i\theta(\alpha, \beta)}}{\int d\alpha d\beta \delta_{N_1, N_2} |\psi(\alpha_2, \beta_1) \psi(\alpha_1, \beta_2) \psi(\alpha_1, \beta_1) \psi(\alpha_2, \beta_2)|}. \quad (\text{S13})$$

In the sign contribution, the angle $\theta(\alpha, \beta)$ is defined as:

$$\exp i\theta(\alpha, \beta) = \frac{\psi(\alpha_1, \beta_2)^* \psi(\alpha_2, \beta_1)^* \psi(\alpha_1, \beta_1) \psi(\alpha_2, \beta_2)}{|\psi(\alpha_1, \beta_2) \psi(\alpha_2, \beta_1) \psi(\alpha_1, \beta_1) \psi(\alpha_2, \beta_2)|}. \quad (\text{S14})$$

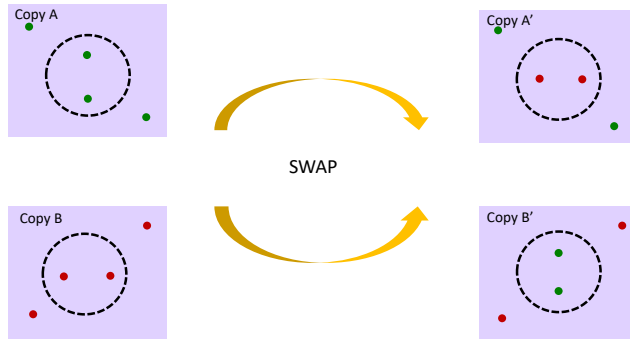


FIG. S5. Illustration of the SWAP process. We have two copies of the full system, whose particles are labeled with different colors, and each copy is divided into two regions separated by the dashed circle. Through the SWAP process, we interchange the particle coordinates inside the circle between the two copies while keeping the outside coordinates unchanged.

The contributions P_{SWAP} , $\langle \text{SWAP}_{\text{mod}} \rangle$, and $\langle \text{SWAP}_{\text{sign}} \rangle$ yield separate contributions to the total Rényi entropy,

$$S_2 = S_{2,p} + S_{2,\text{mod}} + S_{2,\text{sign}}. \quad (\text{S15})$$

In previous works, such as Ref. [28], the first two contributions to the entropy were lumped together, because $S_{2,p} + S_{2,\text{mod}} \equiv S_2(|\Psi|)$ can be interpreted as the entropy of the absolute value of the wave function Ψ . While this may be useful for gapped states [58], our data below suggests this is not helpful for gapless CFL states since $S_{2,p}$ and $S_{2,\text{mod}}$ exhibit different scaling with λ . Hence, we will study individually all three distinct contributions to S_2 .

Mod and sign entropy for free fermions

The scaling of different contributions to entropy in Eq. (S15) is not rigorously known, even for free fermions where the full entropy has an established analytic expression. Fig. S6 contrasts the full S_2 entropy for free fermions [Fig. S6(a)] against its decompositions in Eq. (S15) obtained via Monte Carlo [Fig. S6(b)-(d)]. While the full entropy can be computed for large free-fermion systems containing thousands of particles, the evaluation of mod-sign entropy contributions, to the best of our knowledge, can only be done with Monte Carlo. This limits the accessible system sizes to $N \lesssim 100$, which is similar to the range of system sizes for the CFL states.

Within the range $N \lesssim 100$, we already observe the full entropy S_2 steadily converging to the Widom slope in Fig. S6(a). Figs. S6(b)-(c) illustrate the importance of considering the p and mod contributions to the entropy separately. They each converge nicely to the respective scalings, $S_{2,p} \sim \mathcal{O}(\ln \lambda)$ and $S_{2,\text{mod}} \sim \mathcal{O}(\lambda)$. However, if we add them together to make up $S_2(|\Psi|)$, Fig. S6(c), the latter converges non-monotonically when plotted as $S_2(|\Psi|)/\lambda$ vs $\ln \lambda$. If we estimate the slope of $S_2(|\Psi|)$ by adding the fits, we obtain the solid line in Fig. S6(c), which suggests that our system sizes are not large enough to see the asymptotic area law scaling $S_2(|\Psi|) \sim \lambda$ that we expect in the thermodynamic limit. This has an impact on the scaling of the sign entropy in Fig. S6(d), which overshoots the Widom slope to compensate for the downturn in $S_2(|\Psi|)$. By plotting the Widom slope minus the extrapolation of $S_2(|\Psi|)$ using a solid line in Fig. S6(d), we see that it may only approach the Widom scaling in much larger system sizes ($\ln \lambda \gtrsim 4$). At the same time, the full entropy in Fig. S6(a) tracks the Widom scaling much more closely even in smaller system sizes. As the range of system sizes in this example is comparable to the CFL case, there appears to be little value in considering the mod and sign decompositions over the full entropy.

Mod and sign entropy for CFL

For completeness, in Fig. S7 we compare the full S_2 entropy against its mod-sign decompositions for the four CFL states considered ($\nu=1/m$, $m = 1, 2, 3, 4$). As mentioned in the main text, all of these cases display a significant enhancement of *full* entropy scaling. Mod-sign entropy decompositions, on the other hand, are plagued by similar

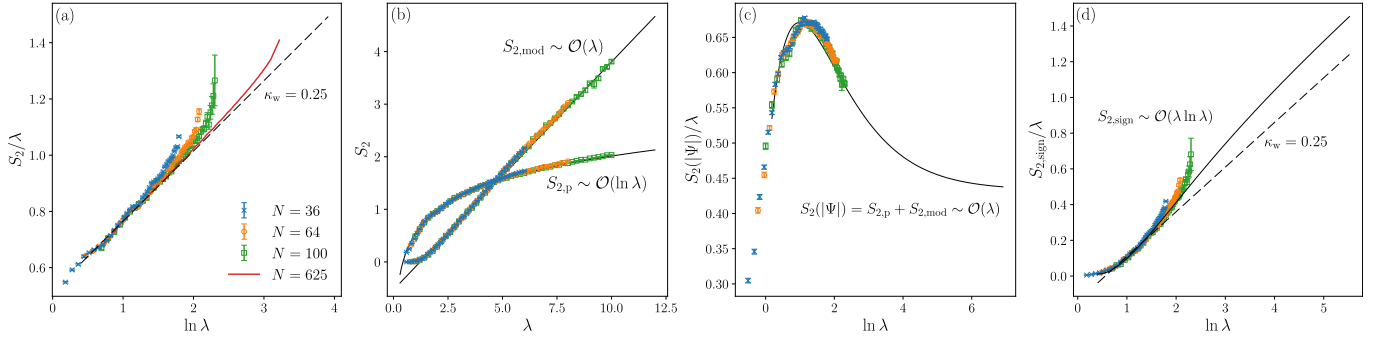


FIG. S6. SWAP decomposition of the S_2 Rényi entropy for free fermions on the sphere. (a) Total S_2 entropy, computed via Monte Carlo (markers), while exact diagonalization result (solid line) is for the largest system size $N = 625$. All system sizes steadily approach the Widom slope $\kappa_w=0.25$ (dashed line). (b): $S_{2,p}$ and $S_{2,mod}$ that make up the absolute value entropy $S_2(|\Psi|)$. $S_{2,p}$, given by the logarithm of the probability that the bipartitions of two copies of the system are swappable, scales logarithmically with the subsystem size. $S_{2,mod}$ appears to follow an area-law growth. Black lines are extrapolations $\lambda \rightarrow \infty$. (c) The absolute value entropy $S_2(|\Psi|) = S_{2,p} + S_{2,mod}$. The black line is the sum of the extrapolations in (b), which eventually settles to an area law for very large systems. However, unlike the individual decompositions in (b), their sum here appears far from the asymptotic scaling regime. (d) The sign entropy $S_{2,sign}$. The dashed line is the Widom slope, while the continuous black line is the Widom slope minus the extrapolation of $S_2(|\Psi|)$, showing the difficulty in extracting the Widom slope solely from the sign term.

issues as the free-fermion case discussed above. For example, in all the cases shown in Fig. S7, the mod contribution to the entropy is still quite large and, in fact, comparable to the sign entropy, which is expected to be the dominant contribution. Similarly, the expected area-law of $S_{2,mod}$, i.e., $S_{2,mod}/\lambda$ becoming flat when plotted as a function of $\ln \lambda$, is not yet reached in Fig. S7. This precludes drawing a clear conclusion based on the isolated sign entropy scaling. One new issue that arises in the CFL case is the large discrepancy between projected and unprojected CFL wave functions. This difference appears to be an artifact of the decomposition, since the full S_2 entropies are essentially unaffected by LLL projection, as we can see from the first panel in each row of Fig. S7.

Flux-attached wave functions

In the main text, we have mentioned the possibility of the Widom formula losing its “universal” geometric character in NFLs, such that the coefficient of the leading term depends on microscopic details of flux attachment. To further explore this, we calculate the Rényi entropy and its decomposition in “flux-attached” wave functions, where the Jastrow factors are replaced by their phases:

$$\Psi_m^{\text{CFL,flux}} = \text{Det}[\chi_n(z_j)] \prod_{i<j} \left(\frac{(z_i - z_j)}{|z_i - z_j|} \right)^m e^{-\frac{1}{4} \sum_k |z_k|^2}. \quad (\text{S16})$$

For such a wave function, the mod entropy is identical to that of free fermions, placing any potential enhancement solely in the sign structure of the wave function.

Figure S8 shows results for $S_{2,sign}$ for the state in Eq. (S16), with $m=2$ in the spherical geometry. We see that the sign entropy is significantly enhanced, even surpassing the standard vortex-attached wave functions discussed in the main text, which is in good agreement with the lattice realization of the flux-attached wave function [77]. Unfortunately, we are unable to efficiently project this wave function, as a significant proportion of it resides outside the lowest Landau level.

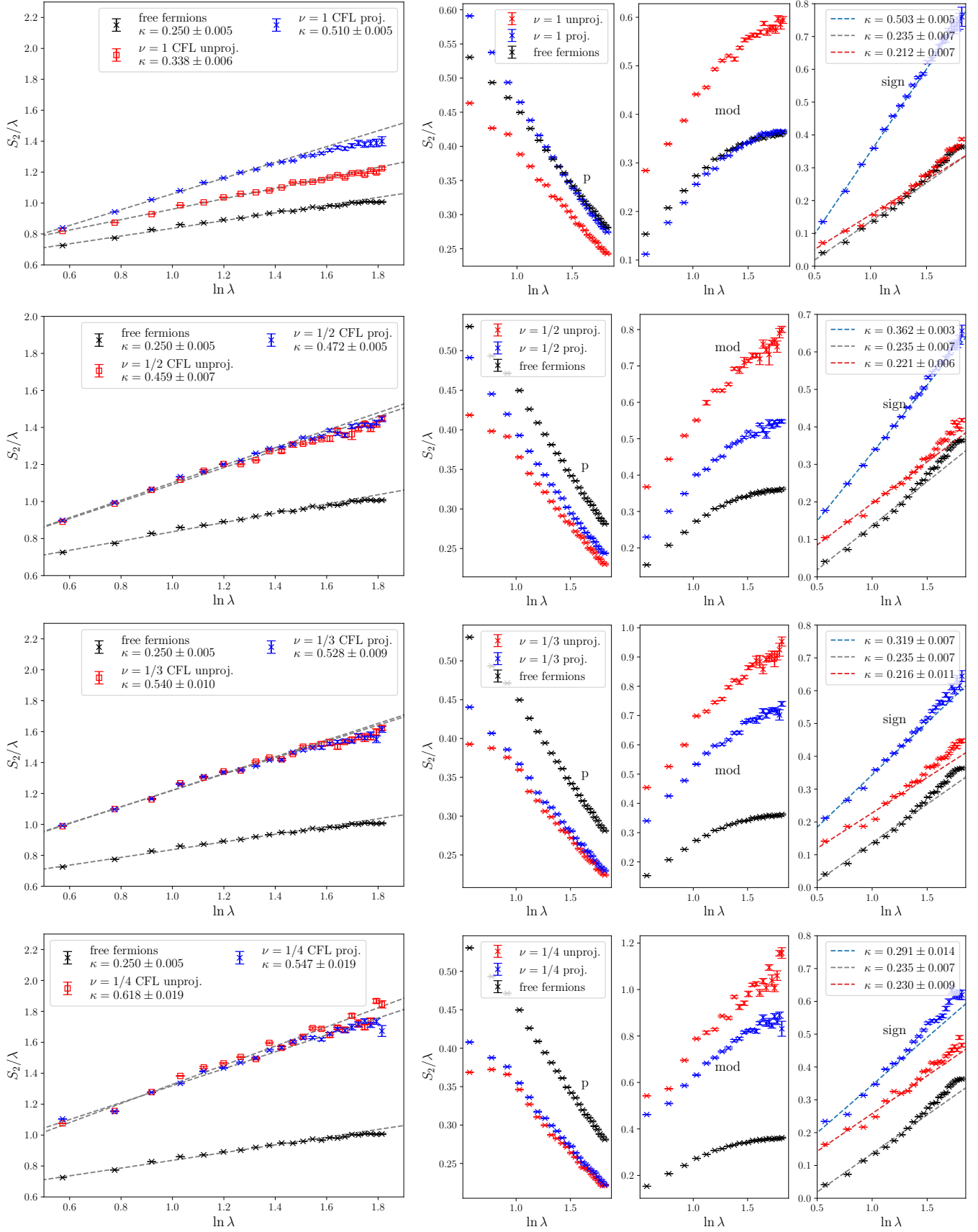


FIG. S7. Entropy decompositions at $\nu = 1$ (first row), $\nu = 1/2$ (second row), $\nu = 1/3$ (third row), and $\nu = 1/4$ (fourth row). Each row contains the data for both the projected and unprojected CFL wave functions on the torus. The first panel in each row shows the total entropy S_2 , which is only affected by the projection in the case of $\nu = 1$. The remaining three panels in each row show the p, mod, and sign contribution to the entropy.

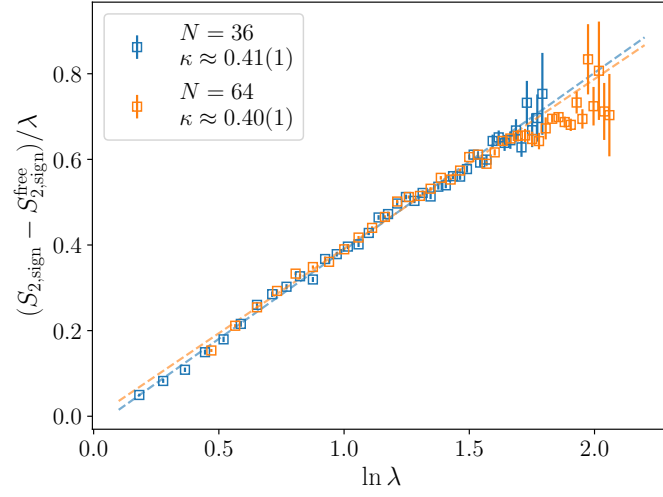


FIG. S8. Difference in sign entropy $S_{2,\text{sign}} - S_{2,\text{sign}}^{\text{free}}$ between the flux-attached CFL at filling $\nu=1/2$ and free fermions, on the sphere. We notice that the entanglement scaling of the sign entropy is considerably enhanced.